Meteoritics & Planetary Science 55, Nr 1, 231–244 (2020)
doi: 10.1111/maps.13423

Report

Characterization of the matrix and fusion crust of the recent meteorite fall Ozerki L6

A. A. MAKSIMOVA[1], E. V. PETROVA[1], A. V. CHUKIN[1], M. S. KARABANALOV[2], I. FELNER[3], M. GRITSEVICH[1,4,5], and M. I. OSHTRAKH[1*]

[1]Institute of Physics and Technology, Ural Federal University, Ekaterinburg 620002, Russian Federation
[2]Institute of Material Science and Metallurgy, Ural Federal University, Ekaterinburg 620002, Russian Federation
[3]Racah Institute of Physics, The Hebrew University, Jerusalem 91904, Israel
[4]Department of Physics, University of Helsinki, Gustaf Hällströmin katu 2a, PO Box 64, FI-00014, Helsinki, Finland
[5]Finnish Geospatial Research Institute, Geodeetinrinne 2, 02430 Masala, Finland
*Corresponding author. E-mail: oshtrakh@gmail.com

(Received 31 May 2019; revision accepted 27 October 2019)

Abstract–We studied the interior and the fusion crust of the recently recovered Ozerki L6 meteorite using optical microscopy, scanning electron microscopy (SEM) with energy dispersive spectroscopy, X-ray diffraction (XRD), magnetization measurements, and Mössbauer spectroscopy. The phase composition of the interior and of the fusion crust was determined by means of SEM, XRD, and Mössbauer spectroscopy. The unit cell parameters for silicate crystals were evaluated from the X-ray diffractograms and were found the same for the interior and the fusion crust. Magnetization measurements revealed a decrease of the saturation magnetic moment in the fusion crust due to a decrease of Fe-Ni-Co alloy content. Both XRD and Mössbauer spectroscopy show the presence of magnesioferrite in the fusion crust. The temperatures of cation equilibrium distribution between the M1 and M2 sites in silicates calculated using the data obtained from XRD and Mössbauer spectroscopy appeared to be in a good consistency: 553 and 479 K for olivine and 1213 and 1202 K for orthopyroxene.

INTRODUCTION

On June 21, 2018 at 01:16:20 UT, an exceptionally bright fireball was witnessed in the Lipetsk Region, Russian Federation as well as in neighboring areas. An analysis of the fireball trajectory, following Lyytinen and Gritsevich (2016) and references therein, was clearly indicative that a number of meteorite fragments survived through atmospheric entry and landed on the ground. A meteorite expedition from the Ural Federal University initiated a meteorite recovery campaign that successfully recovered the first meteorite fragments within 2 days from the fall. The meteorite was classified as ordinary chondrite L6 with a shock stage S4/5 and weathering grade W0 and named Ozerki (Meteoritical Bulletin 2018).

One of the Ozerki L6 meteorite fragments was chosen for the study using optical microscopy, scanning electron microscopy (SEM) with energy dispersive spectroscopy (EDS), X-ray diffraction (XRD), magnetization measurements, and Mössbauer spectroscopy with a high velocity resolution. Additionally, the fusion crust from this fragment was also studied by these techniques.

MATERIALS AND METHODS

The studied Ozerki L6 meteorite fragment is shown in Fig. 1. A thin layer of the fusion crust is present at the fragment's surface. This fragment was cut, and a polished thin section was prepared using the standard method. The polished thin section was then characterized by optical microscopy and SEM with EDS. Then, powdered matter was removed from the polished thin section for further study by means of XRD, magnetization measurements, and Mössbauer spectroscopy. For Mössbauer spectroscopy, a powdered

Fig. 1. Photograph of the studied fragment of Ozerki L6 ordinary chondrite. The fusion crust can be seen on the top of this fragment. (Color figure can be viewed at wileyonlinelibrary.com.)

material was glued onto Al foil free from Fe with a thickness of ~6 mg Fe cm^{-2}. Similarly, a powdered fusion crust was prepared for the study by these techniques.

An Axiovert 40 MAT microscope (Carl Zeiss) was used for optical microscopy characterization of the Ozerki L6 fragment. Scanning electron-ion microscope Auriga CrossBeam (Carl Zeiss) was used for SEM analysis while an EDS device X-max 80 (Oxford Instruments) was applied for the analysis of chemical composition of Ozerki L6. XRD analyses were done on the interior and fusion crust using the XRD-7000 powder diffractometer (Shimadzu) operated at 40 kV and 30 mA with CuK_α radiation using a monochromator, scanned over 2Θ from 12° to 86° with a step of 0.03° per 10 s. The XRD patterns were fitted using PANalytical ′(X'Pert) High Score Plus software with the Rietveld full profile analysis and ICDD PDF2 database. Magnetization measurements were carried out using commercial SQUID MPMS-5S magnetometer (Quantum Design) on a few mg of the powdered samples, in the temperature range of 5–295 K. The differential SQUID sensitivity was 10^{-7} emu. The sample was cooled to 5 K and the field (90 Oe) was switched on to trace the zero-field-cooled (ZFC) branch of the magnetization $M(T)$ curve. The magnetometer was adjusted to be in a real $H = 0$ state prior to recording the ZFC curve. Under this field, the field-cooled (FC) branch was measured via heating from 5 to 295 K.

An automated precision Mössbauer spectrometric system was used for ^{57}Fe Mössbauer spectra measurement. This system was built on the base of the SM-2201 spectrometer operating with a sawtooth shape velocity reference signal. This signal is formed by the digital–analog converter using discretization of 2^{12} (the velocity quantification using 4096 steps). The high level of velocity scale discretization provides much better adjusting to resonance and significantly increases the spectra quality and possibilities to reveal small overlapping spectral components with respect to conventional Mössbauer setups with a considerably lower level of the velocity reference signal discretization. Descriptions of this spectrometer and the system were presented elsewhere (Oshtrakh et al. 2009; Semionkin et al. 2010; Oshtrakh and Semionkin 2013, 2016). The ~1.0×10^9 Bq ^{57}Co(Rh) source (Ritverc GmbH, St. Petersburg, Russian Federation) was used at room temperature. The 295 K Mössbauer spectra were measured in transmission geometry with moving absorber, which excludes parabolic distortion of the spectral base line, and recorded in 4096 channels. For their analysis, the spectra of Ozerki L6 interior and the fusion crust were converted into 1024 channels by a consequent summation of four neighboring channels to increase the signal-to-noise ratio for the minor spectral components. The statistical rates in the spectra were ~9.8×10^6 and ~10.4×10^6 counts per channel and signal-to-noise ratios were 217 and 233 for the powdered internal bulk material and the fusion crust spectra, respectively. Each spectrum was measured for 16 days to reach the signal-to-noise ratio appropriate for reliable fits of the smallest spectral components. Mössbauer spectra were computer fitted with the least squares procedure using UNIVEM-MS program with a Lorentzian line shape. The line shapes of the Mössbauer spectrum of the reference absorber of α-Fe foil (the thickness of ~7 μm) were pure Lorentzian. The line widths (Γ, the full width at a half maximum) in the 1024-channel spectrum of α-Fe foil were $\Gamma_{1,6} = 0.228 \pm 0.030$ mm s^{-1}, $\Gamma_{2,5} = 0.227 \pm 0.030$ mm s^{-1}, and $\Gamma_{3,4} = 0.216 \pm 0.030$ mm s^{-1} for the first and the sixth, the second and the fifth, the third and the fourth peaks in sextet, respectively. Velocity resolution (velocity per one channel) in the 1024-channel Mössbauer spectra was ~0.015 mm s^{-1} per channel for the powdered material and ~0.019 mm s^{-1} per channel for the fusion crust due to the different velocity ranges used for these spectra measurements. The spectral parameters such as: isomer shift, δ, quadrupole splitting, ΔE_Q, quadrupole shift for magnetically split components, ε ($2\varepsilon = \Delta E_Q$), magnetic hyperfine field, H_{eff}, line width, Γ, relative subspectrum (component) area, A, and normalized statistical quality of the fit, χ^2, were determined. Criteria for the best fit were the differential spectrum (the difference between experimental and calculated spectral points), χ^2 values, and physical meaning of parameters. An instrumental (systematic) error for each spectrum point was equivalent to ±0.5 channel (the velocity scale) while that for the hyperfine

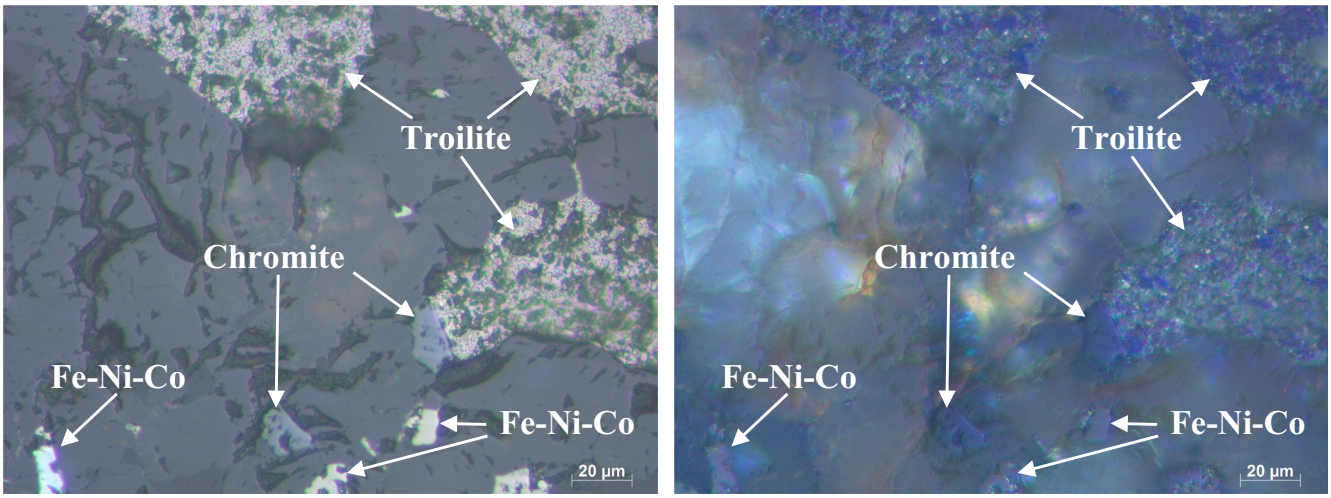

Fig. 2. Selected microphotographs of the polished thin section of Ozerki L6 ordinary chondrite obtained under nonpolarized (left) and polarized (right) light. (Color figure can be viewed at wileyonlinelibrary.com.)

parameters was equivalent to ±1 channel (in mm s^{-1} or kOe). If an error calculated with the fitting procedure (fitting error) for these parameters exceeded the instrumental (systematic) error, the larger error was used instead. The instrumental relative error for A was estimated to be ≤10% (the values of A are given in tables as calculated in the fit with two decimal digits to keep the total relative area equal to 100%). Values of δ are given relative to α-Fe at 295 K.

RESULTS AND DISCUSSION

The Interior

Selected optical microphotographs of the Ozerki L6 polished thin section obtained under nonpolarized and polarized light are shown in Fig. 2. Some phases such as Fe-Ni-Co alloy grains, troilite, and chromite inclusions were found in silicate matrix consisting of olivine and pyroxenes. It was interesting to observe a part of troilite inclusions with a high grade of porosity. Selected SEM images of Ozerki L6 polished thin section are shown in Fig. 3 (additional images can be found in Fig. S1 in supporting information). These images showed the presence of Fe-Ni-Co grains with different α-, α_2-, and γ-phases which differ in the Ni content. Some grains contained 30–33 atom% of Ni that corresponds to the presence of the paramagnetic γ-Fe (Ni, Co) phase. Chromite grains were found with Al as the third largest metal content in addition to Cr and Fe. This means that chromite may contain some part of hercynite ($FeAl_2O_4$) or mixed Al and Cr spinel. Troilite inclusions were observed as homogeneous particles and as particles with a high level of porosity, probably a mixture of troilite with silicate matrix. The content of metals in different minor iron-bearing phases is shown in Table 1.

Analysis of the XRD pattern of the bulk material from Ozerki L6 ordinary chondrite (see Fig. S2 in supporting information) showed the presence of olivine (50.6 wt%), orthopyroxene (23.0 wt%), anorthite (14.4 wt%), troilite (4.5 wt%), Ca-rich clinopyroxene (3.3 wt%), the α-Fe(Ni, Co) phase (1.8 wt%), chromite (1.5 wt%), the γ-Fe(Ni, Co) phase (0.4 wt%), hercynite (0.3 wt%), and chlorapatite $Ca_5(PO_4)_3Cl$ (0.2 wt%). The unit cell parameters were evaluated using the Rietveld full profile analysis for olivine, orthopyroxene, and Ca-rich clinopyroxene found in Ozerki L6 (Table 2).

The $M(T)$ ZFC and FC and $M(H)$ measurements of the bulk material from Ozerki L6 ordinary chondrite are shown in Fig. 4. Two peaks around 18 and 58 K are observed in the ZFC branch. The higher peak is attributed to the ferrimagnetic chromite (Gattacceca et al. 2011) and the peak at 18 K is probably due to hercynite $FeAl_2O_4$ because its Curie temperature (T_C) is around 15 K (Sack and Ghiorso 1991; Klemme and Van Miltenburg 2003; Gattacceca et al. 2011). Both transitions are also observed in the FC branch. Note that the two branches do not merge at 295 K, indicating other magnetic phase(s) which order well above room temperature.

The isothermal magnetization $M(H)$ curves of Ozerki L6 measured at 5 and 295 K up to 45,000 Oe are also depicted in Fig. 4. In both cases, $M(H)$ first increases linearly up to 3000–4000 Oe and then tends to saturate. The $M(H)$ plots clearly reveal an admixture of at least two components and can be fitted as: $M(H) = M_S + \chi_p H$, where M_S corresponds to the intrinsic magnetic saturation moment and $\chi_p H$ is the linear paramagnetic part. At 5 and 295 K, the M_S values are

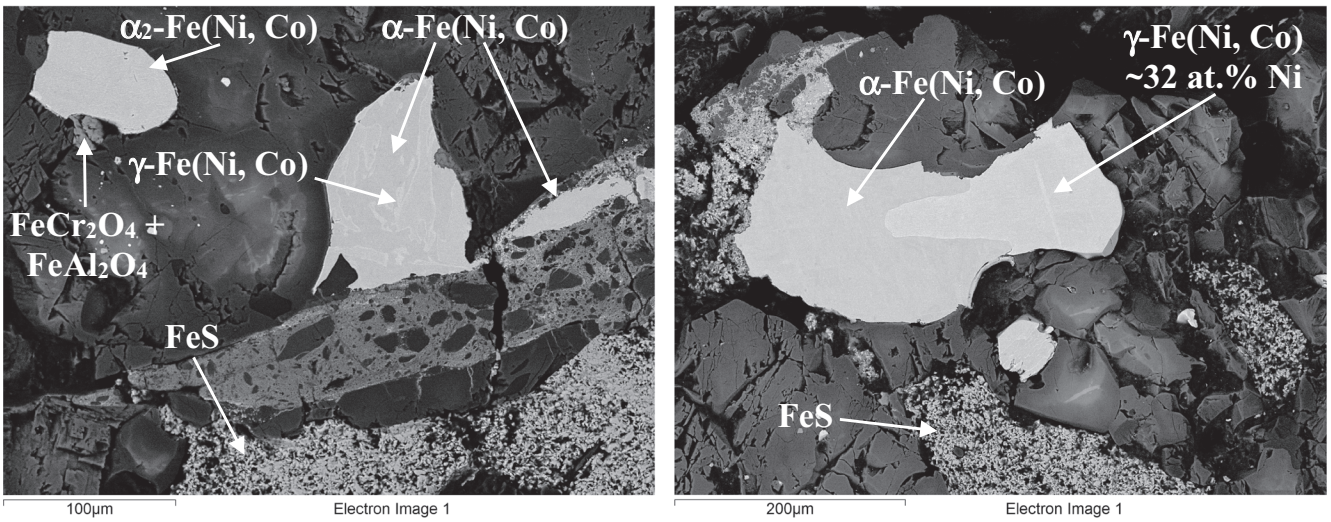

Fig. 3. Selected scanning electron microscopy images of the polished thin section of Ozerki L6 ordinary chondrite. Indicated phases were determined using energy dispersive spectroscopy (see also Fig. S1).

Table 1. Averaged ranges of metals in selected minor iron-bearing phases in the polished thin section of Ozerki L6 ordinary chondrite obtained using energy dispersive spectroscopy.

Minor phases	wt%
α-Fe(Ni, Co)	
Fe	92.2–95.3
Ni	2.8–6.0
Co	1.6–2.9
α_2-Fe(Ni, Co)	
Fe	74.6–86.2
Ni	12.0–23.8
Co	1.8–2.5
γ-Fe(Ni, Co)	
Fe	49.5–63.7 69.4–71.4
Ni	27.2–28.2 34.9–49.4
Co	0.5–2.4
γ-Fe(Ni, Co) par	
Fe	66.0–69.4
Ni	29.0–33.1
Co	1.4–1.9
$FeCr_2O_4$	
Fe	9.3–9.8
Cr	15.6–17.4
Al	2.9–3.0
Ti	0.8–1.0
Mg	1.3–1.6
Mn	0.8–0.9

"Par" means the paramagnetic state of the γ-phase.

51.1 and 46.7 emu per g, respectively, and related to Fe-Ni-Co alloy (see Gattacceca et al. 2014). The slight loss in the saturation moments (8.6%) indicates that this alloy in Ozerki L6 orders at elevated temperatures. That is consistent with the shown $M(T)$ plots.

Table 2. The unit cell parameters for silicate crystals in the bulk interior of Ozerki L6 ordinary chondrite obtained from X-ray diffraction.

	Unit cell parameters			
Silicate crystals	*a* (Å)	*b* (Å)	*c* (Å)	β (°)
Olivine	10.271 (3)	6.012 (3)	4.772 (2)	–
Orthopyroxene	18.276 (4)	8.867 (3)	5.207 (3)	–
Ca-rich clinopyroxene	9.75 (5)	8.90 (4)	5.28 (4)	106.1

Mössbauer spectrum of the bulk material of Ozerki L6 ordinary chondrite is shown in Fig. 5. This spectrum is similar to other L ordinary chondrites (see Maksimova and Oshtrakh (2019) and references therein). To fit this spectrum well, we used an approach to simulate the full static Hamiltonian to fit troilite component in the complex Mössbauer spectra of ordinary chondrites that was described in detail by Maksimova et al. (2014a, 2016, 2017) and Oshtrakh et al. (2016). We also accounted for spectral components related to the ^{57}Fe in the M1 and M2 sites in silicate crystals and different phases for Fe-Ni-Co alloy as well as to components associated with chromite and hercynite for the fitting model. The result of the best fit is shown in Fig. 5. The obtained Mössbauer parameters for spectral components are given in Table 3. The assigning of spectral hyperfine parameters to the indicated compounds (phases) was done in the same way as it was recently done in the studies of other ordinary chondrites (see Maksimova et al. 2018b; Oshtrakh et al. 2019; and references therein). It should be noted that we were unable to calculate correctly the

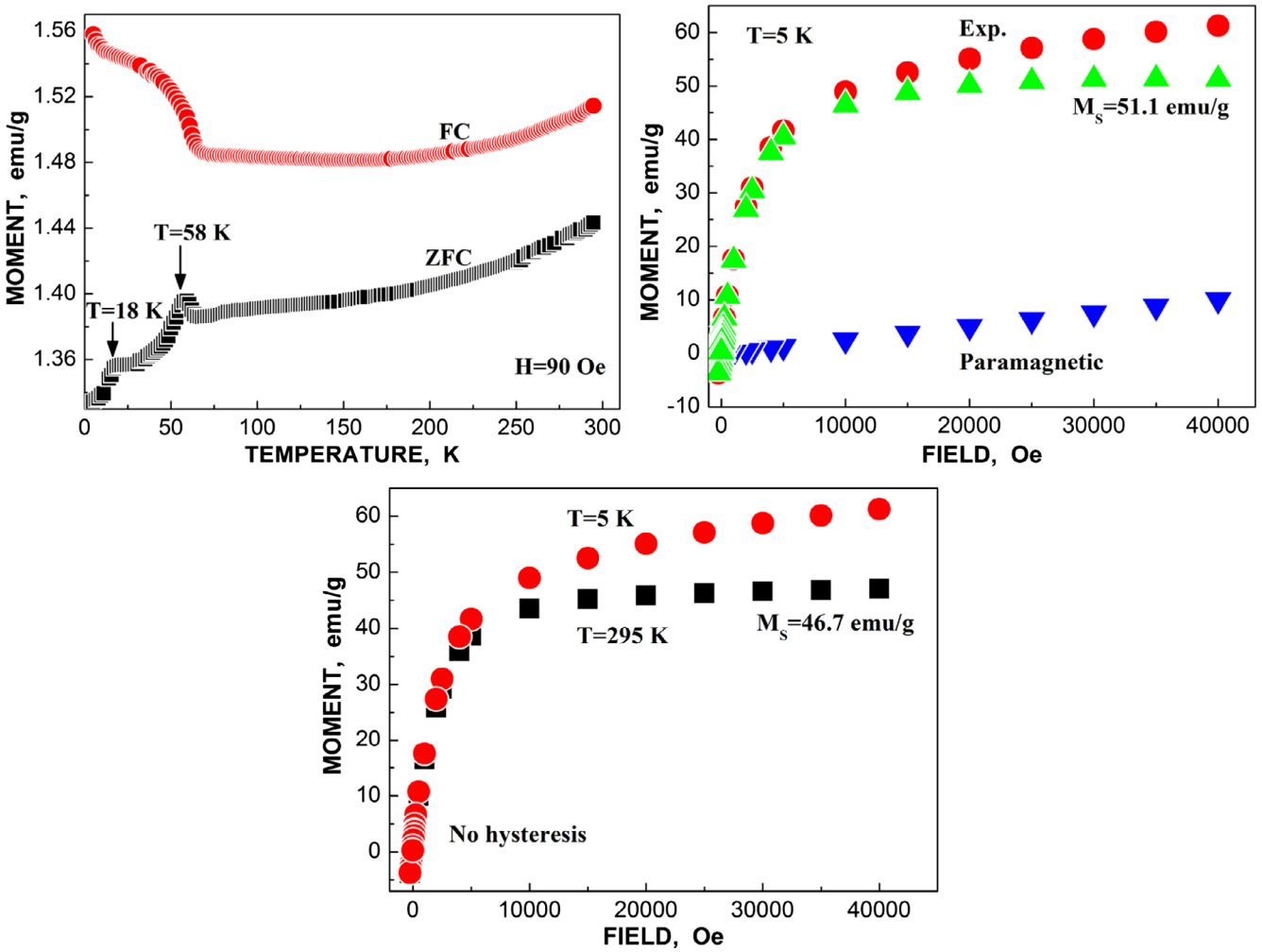

Fig. 4. Zero-field-cooled (ZFC) and field-cooled (FC) magnetization curves and isothermal magnetization curves of the bulk interior of Ozerki L6 fragment. Exp. = experimental points, M_S = saturation magnetic moment, T = temperature. (Color figure can be viewed at wileyonlinelibrary.com.)

spectral components which could be assigned to the M1 and M2 sites in clinopyroxene. This is a result of a very low content of clinopyroxene (XRD showed the presence of ~3 wt% of clinopyroxene). In case of a low content of clinopyroxene, its low-intensity spectral components overlapping with high-intensity spectral components of orthopyroxene cannot be revealed well without significant increase in correlation of their parameters. The same was found in the case of the Mössbauer spectrum of Chelyabinsk LL5 fragment no. 1 with the presence of 3.9 wt% of clinopyroxene. In the other Chelyabinsk fragments that had larger clinopyroxene content, these components were revealed in the Mössbauer spectra (Oshtrakh et al. 2019).

If we assume the same Mössbauer effect probability (the f-factor) for all phases in Ozerki L6, we can roughly estimate the iron fraction in all iron-bearing minerals (by using relative areas of spectral components) and compare with some recently studied ordinary chondrites Northwest Africa 6286 LL6, Chelyabinsk LL5 (fragments no. 1 and no. 2), and Tsarev L5 (Maksimova et al. 2018a, 2018b; Oshtrakh et al. 2019). For example, the metal content in Ozerki L6 is slightly larger than that for the three LL chondrites. Following the assumption about the same f-factor for all phases, we can roughly estimate the Fe^{2+} fractions (occupancies) in the M1 and M2 sites (X_{Fe}^{M1} and X_{Fe}^{M2}) in silicate crystals in Ozerki L6 meteorite. The ratios of X_{Fe}^{M1}/X_{Fe}^{M2} are equal to the corresponding ratios of the subspectra relative areas A^{M1}/A^{M2}. The Rietveld full profile analysis can obtain directly the X_{Fe}^{M1} and X_{Fe}^{M2} from the Ozerki L6 XRD pattern. Therefore, it is possible to compare X_{Fe}^{M1}/X_{Fe}^{M2} for olivine and orthopyroxene using two independent techniques (see Table 4). A good consistency of X_{Fe}^{M1}/X_{Fe}^{M2} values obtained using the data from XRD and A^{M1}/A^{M2} values from Mössbauer spectroscopy is clearly seen in Table 4.

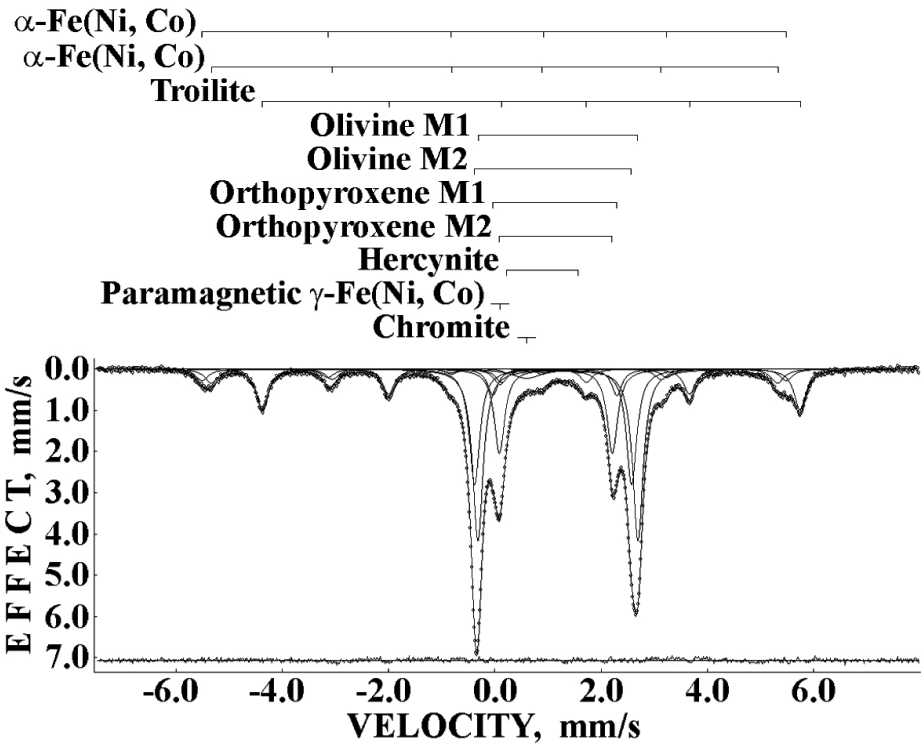

Fig. 5. Mössbauer spectrum of the bulk interior of Ozerki L6 fragment. Indicated components are the results of the best fit. The differential spectrum is shown below. T = 295 K.

The distribution of Fe^{2+} and Mg^{2+} cations between the M1 and M2 sites in orthopyroxene and, probably, in olivine is related to the minerals' thermal history. Using the distribution coefficient $K_D = (X_{Fe}{}^{M1} \times X_{Mg}{}^{M2})/(X_{Fe}{}^{M2} \times X_{Mg}{}^{M1})$, it is possible to determine the temperature of equilibrium cation distribution T_{eq}. The Fe^{2+} and Mg^{2+} occupancies were determined from XRD (see Table 4, $X_{Fe}{}^{M1} + X_{Mg}{}^{M1} = 1$). Therefore, the values of K_D for olivine and orthopyroxene that were calculated from these data are 1.58 and 0.24, respectively. To determine T_{eq}, we used equations for olivine: $-\Delta G^\circ = R \times T_{eq} \times \ln K_D$, where the Gibbs energy ΔG° = 20,935 J for olivine, R = 8.31 J K mol^{-1} (Malysheva 1975), and for orthopyroxene: $\ln K_D = 0.391–2205/T_{eq}$ (Wang et al. 2005). Calculated values of T_{eq} are 553 and 1213 K for olivine and orthopyroxene, respectively. Using relative areas of corresponding spectral components in the Mössbauer spectrum of Ozerki L6, we can calculate K_D and T_{eq} for olivine and orthopyroxene also using the values of fayalite (Fa) and ferrosilite (Fs) for this meteorite by means of approach described in detail by Oshtrakh et al. (2008, 2019). The values of Fa and Fs are 0.26 and 0.21 (Meteoritical Bulletin 2018). The values of K_D and T_{eq} calculated from Mössbauer data are 1.69 and 479 K for olivine and 0.24 and 1202 K for orthopyroxene. The results obtained using two independent techniques are in a good consistency. Moreover, the values of T_{eq} calculated by two techniques for orthopyroxene in Ozerki L6 agree with the T_{eq} range of 1085–1207 K calculated by Slater-Reynolds and McSween (2005) for orthopyroxene in L6 ordinary chondrites.

The relative areas of components in the Mössbauer spectra of ordinary chondrites can be used for meteorites classification as has already been shown by Paliwal et al. (2000), Verma et al. (2002, 2003), Verma and Tripathi (2004), Oshtrakh et al. (2008), Galazka-Friedman et al. (2017), and Elewa and Cadogan (2017). We used this approach also and found that the plot of the total relative area of components related to Fe-Ni-Co alloy plus those assigned to Fe^{3+} compounds versus the total relative area of components associated with the M1 and M2 sites in olivine can be considered as the most useful for classification (Oshtrakh et al. 2008, 2019; Maksimova et al. 2017, 2018b; Maksimova and Oshtrakh 2019). This way is possible for nonweathered meteorites and in situations with small weathering grade when iron in silicate crystals is not oxidized. In the plot shown in Fig. 6 for ordinary chondrites from H, L, and LL groups studied in the above-mentioned papers, Ozerki L6 falls in the L ordinary chondrites region.

Table 3. Mössbauer parameters obtained for the Ozerki L6 bulk interior.

Γ (mm s^{-1})	δ (mm s^{-1})	$\Delta E_Q/2\varepsilon$ (mm s^{-1})	H_{eff}, kOe	A (%)	Component[a]
0.296 ± 0.030	0.018 ± 0.015	–0.060 ± 0.015	341.5±0.5	5.10	α-Fe(Ni, Co)
0.296 ± 0.030	0.014 ± 0.015	–0.039 ± 0.015	331.0±0.5	6.26	α-Fe(Ni, Co)
0.275 ± 0.030	0.774 ± 0.015	ND	314.4±0.5	15.83	Troilite
0.234 ± 0.030	1.186 ± 0.015	3.005 ± 0.015	–	29.35	Olivine M1
0.234 ± 0.030	1.096 ± 0.015	2.948 ± 0.015	–	19.83	Olivine M2
0.234 ± 0.030	1.129 ± 0.015	2.331 ± 0.015	–	4.53	Orthopyroxene M1
0.234 ± 0.030	1.148 ± 0.015	2.120 ± 0.015	–	14.42	Orthopyroxene M2
0.234 ± 0.030	0.900 ± 0.018	1.347 ± 0.037	–	0.66	Hercynite
0.689 ± 0.060	0.598 ± 0.022	–	–	2.35	Chromite
0.296[b]	0.102 ± 0.015	–		1.68	Paramagnetic γ-Fe(Ni, Co)

ND = nondetermined.
[a]Components correspond to the spectral components shown in Fig. 5.
[b]Fixed parameter.

Table 4. The ratios of Fe^{2+} occupancies in the M1 and M2 sites in olivine and orthopyroxene microcrystals in the bulk interior of Ozerki L6 ordinary chondrite calculated using X-ray diffraction and Mössbauer spectroscopy data.

	Method of estimation			
	XRD			Mössbauer spectroscopy
Silicate crystals	X_{Fe}^{M1}	X_{Fe}^{M2}	X_{Fe}^{M1}/X_{Fe}^{M2}	A_{Fe}^{M1}/A_{Fe}^{M2}
Olivine	0.27	0.19	1.42	1.48
Orthopyroxene	0.11	0.34	0.32	0.31

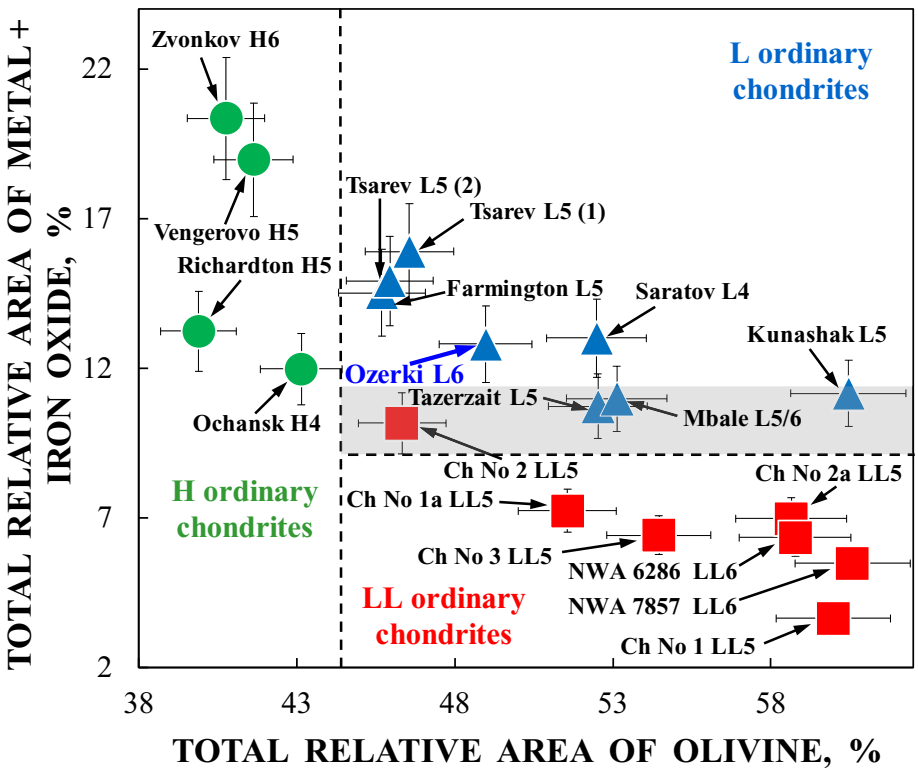

Fig. 6. Systematics of H, L, and LL ordinary chondrites using Mössbauer parameters with position for Ozerki L6 fragment. Abbreviations "Ch" and "NWA" mean "Chelyabinsk" and "Northwest Africa," respectively. Vertical and horizontal error bars are roughly estimated averaged relative errors. Adopted from Oshtrakh et al. (2019). (Color figure can be viewed at wileyonline library.com.)

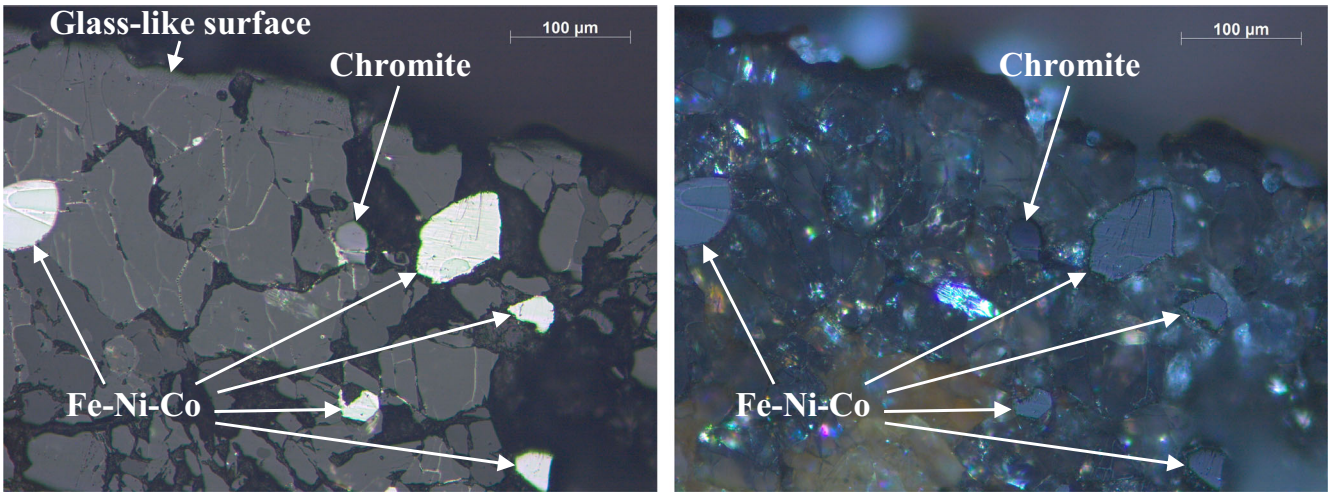

Fig. 7. Selected microphotographs of the fusion crust at the polished thin section of Ozerki L6 ordinary chondrite obtained under nonpolarized (left) and polarized (right) light (the higher magnification images of the glass-like surface are shown in Fig. S3). (Color figure can be viewed at wileyonlinelibrary.com.)

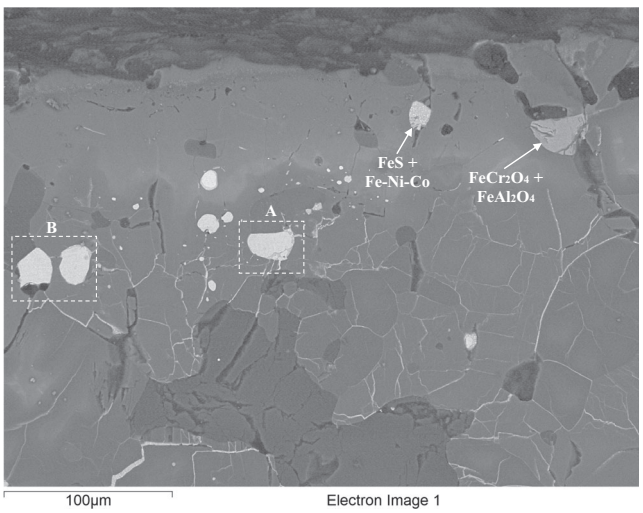

Fig. 8. Scanning electron microscopy image of the fusion crust at the polished thin section of Ozerki L6 ordinary chondrite. Indicated phases were determined using energy dispersive spectroscopy. Areas A and B are shown in Fig. S4 and the glass-like surface is shown in Fig. S5 with high magnifications in supporting information.

The Fusion Crust

The fusion crust can be seen in Fig. 1 at the surface of Ozerki L6 fragment. Microphotographs of this fusion crust obtained under nonpolarized and polarized light are shown in Fig. 7 (microphotographs of the glass-like surface with higher magnification are shown in Fig. S3 in supporting information). These microphotographs showed the glass-like crust surface and the second and the third crust layers (see Rubin 1997) with inclusions of the Fe-Ni-Co grains and chromite particles. SEM images of the Ozerki L6 fusion crust (Fig. 8) also demonstrate the glass-like surface, the second (intermediate) and the third (inner) crust layers with inclusions of the troilite–Fe-Ni-Co grain associations and chromite. The third layer contains many troilite–Fe-Ni-Co veins (Figs. 8 and S4 in supporting information) resulting from rapidly solidified FeS and Fe-Ni-Co alloy intergrowth (Rubin 1997). The glass-like surface shows the formation of fractal-like dendritic crystals (Fig. S5 in supporting information) which indicate rapid solidification of the molten matter in the crust. EDS analysis showed that (1) dendritic crystals consist of silicates like pyroxene with a higher Fe content (~5–10 atom%) and a smaller Mg content (~10–6 atom%), (2) chromite contains ~3 atom% of Al as the third metal after Cr and Fe that indicates the possible presence of hercynite in chromite crystals, (3) troilite consists of ~55–52 atom% of S and ~45–48 atom% of Fe, (4) metal grains consist of the α-Fe (Ni, Co) phase with Ni and Co contents of ~3 and ~2 atom%, respectively, and the α_2-Fe(Ni, Co) phase with Ni and Co contents of ~14 and ~2–2.5 atom%, respectively.

XRD pattern of the Ozerki L6 fusion crust is shown in Fig. 9. This pattern was fitted using the Rietveld full profile analysis which determined the following composition of the crust: olivine (58.8 wt%), orthopyroxene (14.8 wt%), magnesioferrite $MgFe_2O_4$ (13.1 wt%), anorthite (7.6 wt%), troilite (2.0 wt%), Ca-rich clinopyroxene (1.6 wt%), the α-Fe(Ni, Co) phase (1.0 wt%), chromite (0.5 wt%), hercynite (0.4 wt%), and the γ-Fe(Ni, Co) phase (0.2 wt%). The unit cell parameters for silicate crystals in the fusion crust were

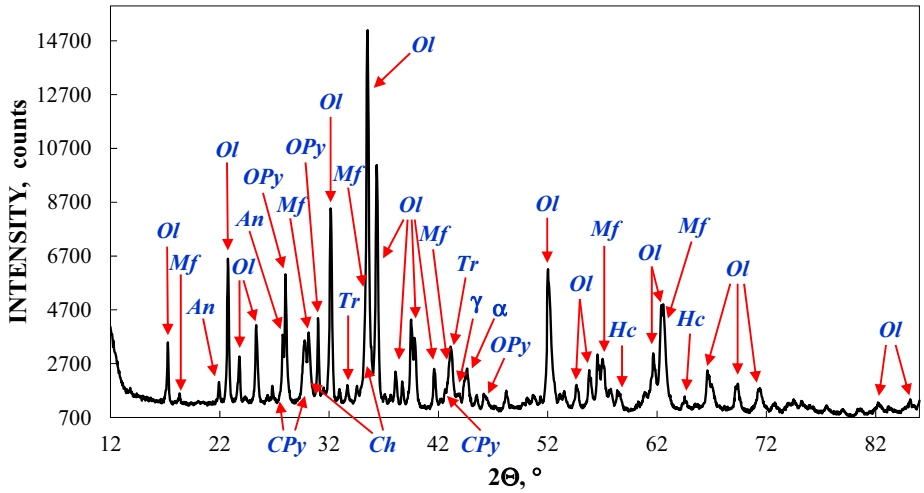

Fig. 9. X-ray diffraction pattern of the fusion crust from Ozerki L6 ordinary chondrite. Ol = olivine, An = anorthite, OPy = orthopyroxene, CPy = clinopyroxene, Tr = troilite, Ch = chromite, Hc = hercynite, Mf = magnesioferrite, α = α-Fe(Ni, Co) phase, γ = γ-Fe(Ni, Co) phase. (Color figure can be viewed at wileyonlinelibrary.com.)

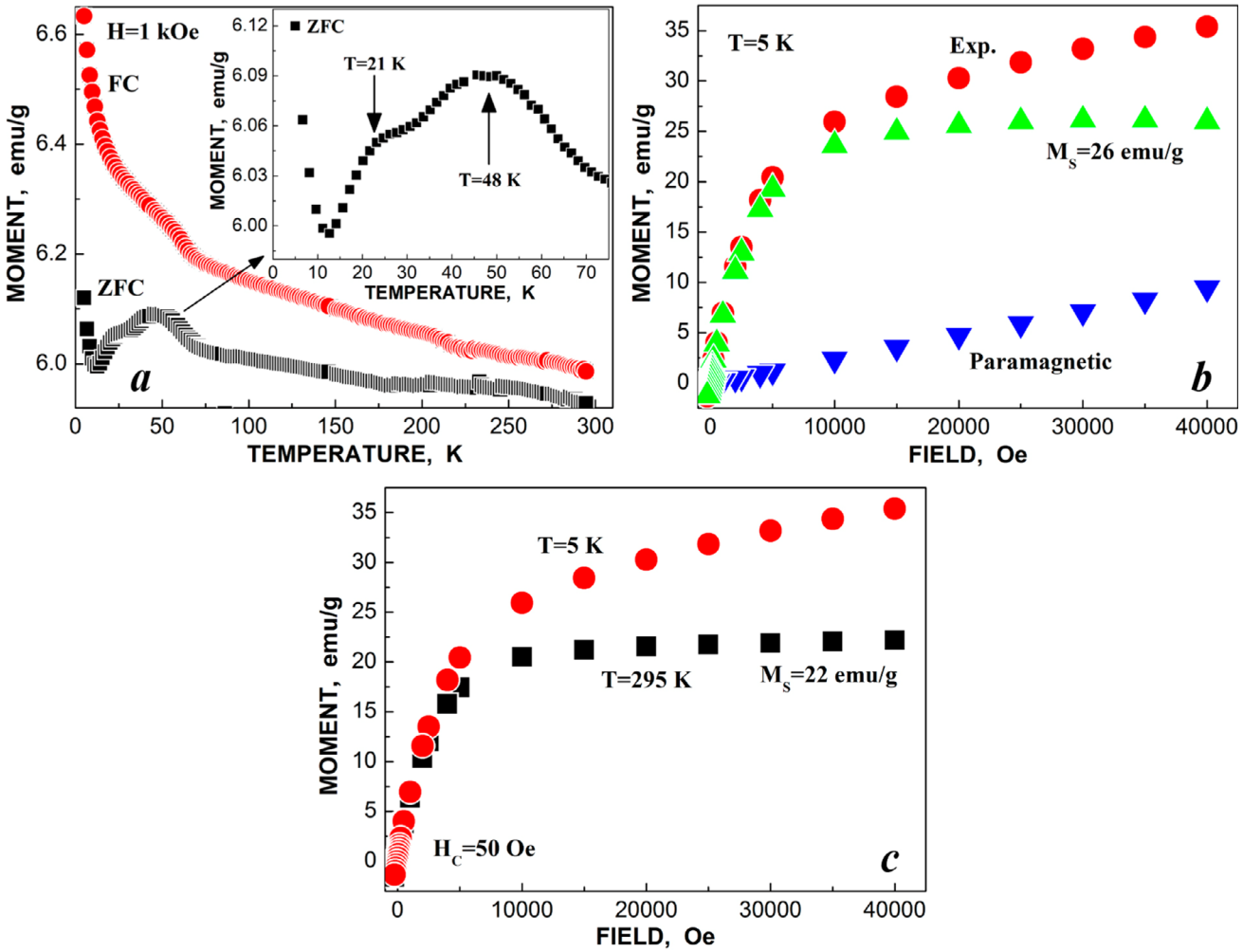

Fig. 10. Zero-field-cooled (ZFC) and field-cooled (FC) magnetization curves and isothermal magnetization curves of the fusion crust of Ozerki L6 fragment. Exp. = experimental points, M_S = saturation magnetic moment, T = temperature. (Color figure can be viewed at wileyonlinelibrary.com.)

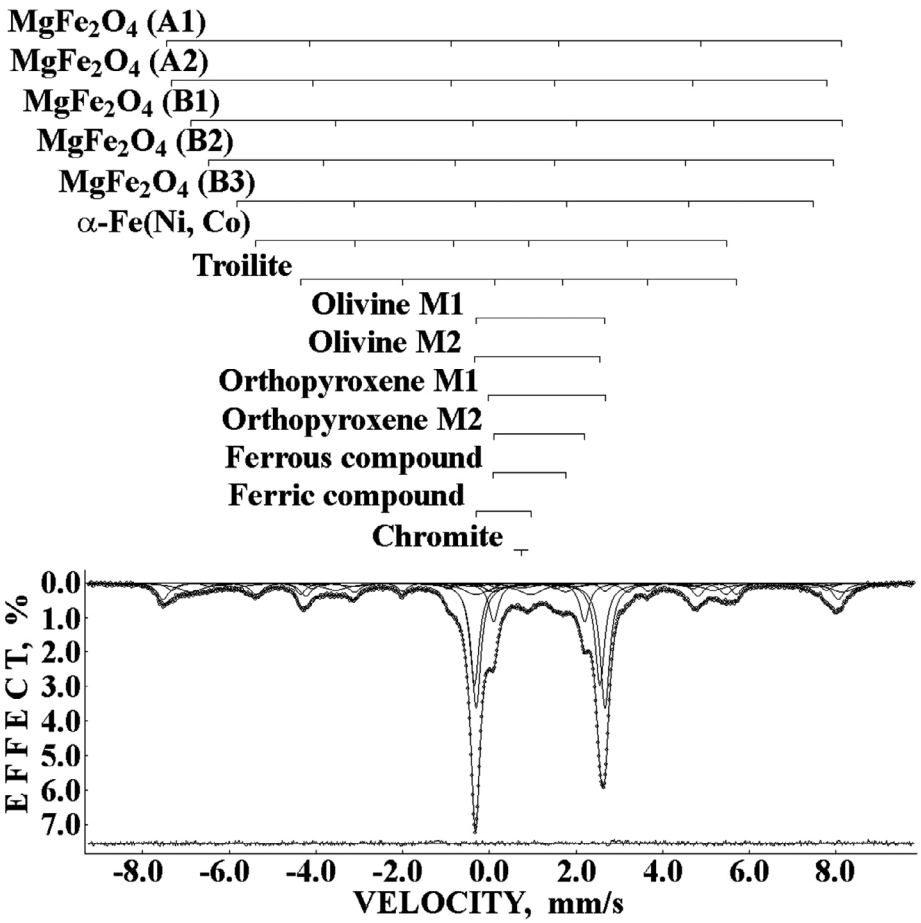

Fig. 11. Mössbauer spectrum of the fusion crust of Ozerki L6 fragment. Indicated components are the results of the best fit. The differential spectrum is shown below. T = 295 K.

Table 5. Mössbauer parameters obtained for the Ozerki L6 fusion crust.

Γ (mm s^{-1})	δ (mm s^{-1})	$\Delta E_Q/2\varepsilon$ (mm s^{-1})	H_{eff}, kOe	A (%)	Component[a]
0.329 ± 0.030	0.277 ± 0.015	–0.026 ± 0.015	484.0 ± 0.5	8.22	$MgFe_2O_4$ (A1)
0.317 ± 0.043	0.271 ± 0.015	–0.078 ± 0.015	469.4 ± 1.0	3.56	$MgFe_2O_4$ (A2)
0.747 ± 0.055	0.721 ± 0.016	–0.188 ± 0.023	467.0 ± 0.9	9.78	$MgFe_2O_4$ (B1)
0.318 ± 0.067	0.538 ± 0.020	0.373 ± 0.036	447.7 ± 1.6	1.51	$MgFe_2O_4$ (B2)
0.776 ± 0.078	0.781 ± 0.021	0.089 ± 0.045	413.4 ± 1.6	4.62	$MgFe_2O_4$ (B3)
0.348 ± 0.030	0.041 ± 0.015	0.003 ± 0.015	337.2 ± 0.5	6.08	α-Fe(Ni,Co)
0.269 ± 0.030	0.773 ± 0.015	ND	312.2 ± 0.5	4.62	Troilite
0.262 ± 0.030	1.183 ± 0.015	2.966 ± 0.015	–	23.69	Olivine M1
0.262 ± 0.030	1.104 ± 0.015	2.887 ± 0.015	–	19.35	Olivine M2
0.262 ± 0.030	1.327 ± 0.016	2.689 ± 0.035	–	1.57	Orthopyroxene M1
0.262 ± 0.030	1.150 ± 0.015	2.091 ± 0.015	–	7.36	Orthopyroxene M2
0.495 ± 0.071	0.927 ± 0.038	1.665 ± 0.067	–	3.05	Ferrous compound
0.656 ± 0.058	0.325 ± 0.023	1.269 ± 0.051	–	5.23	Ferric compound
0.778 ± 0.401	0.748 ± 0.065	–	–	1.37	Chromite

ND = nondetermined.
[a]Components correspond to the spectral components shown in Fig. 11.

the same as those for silicate crystals in the bulk material shown in Table 2. A large amount of magnesioferrite was observed in the fusion crust of Ozerki L6 similar to that found by XRD in the fusion crust from Saratov L4 and two fragments of Chelyabinsk LL5 ordinary chondrites (Yudin et al.

Table 6. The ratios of Fe^{2+} occupancies in the M1 and M2 sites in olivine and orthopyroxene microcrystals in the fusion crust of Ozerki L6 ordinary chondrite calculated using X-ray diffraction and Mössbauer spectroscopy data.

	Method of estimation			
	XRD			Mössbauer spectroscopy
Silicate crystals	X_{Fe}^{M1}	X_{Fe}^{M2}	X_{Fe}^{M1}/X_{Fe}^{M2}	A_{Fe}^{M1}/A_{Fe}^{M2}
Olivine	0.25	0.21	1.19	1.22
Orthopyroxene	0.08	0.36	0.22	0.21

1968; Maksimova et al. 2014b, 2016, 2017; Oshtrakh et al. 2019). In contrast, the majority of previous studies observed magnetite Fe_3O_4 and wüstite FeO in the fusion crust (Rubin 1997). However, according to PDF 01-089-6188, two main magnesioferrite peaks [2 2 0] and [3 1 1] are clearly seen in Fig. 11 at 2Θ ~30° and ~35.5°, respectively.

The results of magnetization measurements of the fusion crust (Fig. 10) seem to be very similar to that of Ozerki L6's interior shown in Fig. 4. Generally speaking, fusion crust material also contains a mixture of a few magnetic and paramagnetic phases, but with different relative fractions, namely that paramagnetic phase(s) are more dominant. That is readily expressed in (1) the uprise of the ZFC curve below 12 K and (2) in the lower M_S values, 26 and 22 emu per g at 5 and 295 K, respectively. That indicates that the magnetic Fe-Ni-Co alloy fraction (with T_C is well above room temperature) is about 50% lower than those obtained for the internal material (Fig. 4), a consequence which confirms the XRD data. We may attribute the broad peaks around 21 and 48–50 K observed in the ZFC branch (Fig. 10, inset) to the same magnetic hercynite and chromite phases as considered above for the interior.

The Mössbauer spectrum of the fusion crust from Ozerki L6 meteorite is shown in Fig. 11. This spectrum demonstrates similar shape as that of the spectra of the fusion crust from Chelyabinsk LL5 fragments (Oshtrakh et al. 2019). This spectrum was fitted well using seven magnetic sextets, six quadrupole doublets, and one paramagnetic singlet. Parameters of these components are shown in Table 5. Based on the hyperfine parameters, these components were related to corresponding compounds (phases). Two magnetic sextets with H_{eff} of ~337 and ~312 kOe are related to the α-Fe(Ni, Co) phase and troilite, respectively. The other five magnetic sextets were associated with magnesioferrite, which has a spinel structure with Fe^{3+} and Mg^{2+} cations in both tetrahedral (A) and octahedral [B] sites within the formula: $(Mg_{1-x}Fe_x)_A[Mg_yFe_{2-y}]_BO_4$. There are eight metal ions in the (A) sites and 16 metal ions in the [B] sites. Therefore, there is a distribution of different numbers of Fe^{3+} and Mg^{2+} cations in the neighboring coordination spheres of ^{57}Fe in both (A) and [B] sites. This leads to different hyperfine fields on the ^{57}Fe nuclei resulting from these distributions. Two magnetic sextets with δ values of about 0.27 mm s^{-1} were assigned to the (A) sites while three magnetic sextets with larger δ values were related to the [B] sites. For example, earlier, De Grave et al. (1979) showed that the Mössbauer spectrum of magnesioferrite can be fitted using one magnetic sextet for the (A) sites and three magnetic sextets for the [B] sites.

Two pairs of quadrupole doublets were assigned to the M1 and M2 sites in olivine and orthopyroxene, respectively, similar to that in the spectrum of bulk material. Two residual quadrupole doublets demonstrate hyperfine parameters corresponding to ferrous and ferric compounds; however, these compounds were not identified yet. These compounds may be a result of structural modification of silicate crystals with partial oxidation during combustion at the atmosphere. Singlet component has parameters corresponding to chromite. The relative part of Fe-Ni-Co alloy in the fusion crust was found by Mössbauer spectroscopy half that in the interior. This is in agreement with XRD data and difference for the saturation magnetic moment for the fusion crust and interior of Ozerki L6 meteorite.

Following the above-mentioned comparison of the M1 and M2 site occupancies by Fe^{2+} and their ratios for olivine and orthopyroxene calculated from XRD and Mössbauer spectra data, we carried out this comparison for silicate crystals in the fusion crust of Ozerki L6 meteorite. These results are given in Table 6. The ratios X_{Fe}^{M1}/X_{Fe}^{M2} and A^{M1}/A^{M2} are in a good consistency for olivine and orthopyroxene, respectively, but these values are slightly lower than those calculated for the bulk material (see Table 4). It is well known that annealing of silicate crystals followed by quenching leads to redistribution of Fe^{2+} and Mg^{2+} cations between the M1 and M2 sites (see, for example, Heinemann et al. 1999; Zema et al. 1999; Morozov et al. 2005). Therefore, we can calculate a temperature T_{FC} similarly to T_{eq} for olivine and orthopyroxene underwent high temperature effect during the fusion crust formation using the

approach applied above for silicates in the interior. The calculated T_{FC} values are as follows: 1113 K (XRD) and 927 K (Mössbauer spectroscopy) for olivine and 978 K (XRD) and 962 K (Mössbauer spectroscopy) for orthopyroxene. These values are very close and if the calculated temperature can be considered as a temperature of silicate crystals annealing during the final layer of the fusion crust formation, both olivine and orthopyroxene were undergone by heating around 1000 K with fast cooling.

CONCLUSIONS

We have studied the sample of the Ozerki L6 meteorite by means of optical microscopy, SEM with EDS, XRD, magnetization measurements, and Mössbauer spectroscopy. The main iron-bearing phases such as olivine, orthopyroxene, troilite, Ca-rich clinopyroxene, α-Fe(Ni, Co) and γ-Fe(Ni, Co) phases, chromite, and hercynite were observed using EDS and XRD in the bulk material. Magnetization measurements demonstrated the magnetic phase transitions of chromite and probably hercynite at 58 and 18 K, respectively. The saturation magnetic moment at 5 K is ~51 emu per g and related to the Fe-Ni-Co alloy mainly, which orders magnetically well above room temperature. Components assigned to the M1 and M2 sites in olivine and orthopyroxene, troilite, the ferromagnetic α-Fe(Ni, Co) and paramagnetic γ-Fe(Ni, Co) phases, chromite, and hercynite were revealed from the Mössbauer spectrum of Ozerki L6. Determination of the Fe^{2+} occupancies of the M1 and M2 sites in both olivine and orthopyroxene by two independent techniques, XRD and Mössbauer spectroscopy, showed a good agreement. The temperatures of cation equilibrium distribution in silicate phases, calculated based on the data from these two techniques, were 553 K (XRD) and 479 K (Mössbauer spectroscopy) for olivine and 1213 K (XRD) and 1202 K (Mössbauer spectroscopy) for orthopyroxene. Systematics of ordinary chondrites using the relative areas of Mössbauer spectral components demonstrated that Ozerki L6 corresponds to the L ordinary chondrites region.

The study of the Ozerki L6 fusion crust by the same techniques demonstrated the following. The fusion crust consists of three layers of glass-like, molten, and partially molten silicate phases with grains of chromite, Fe-Ni-Co alloy, and veins of FeS–Fe-Ni-Co alloy intergrowth resulting from rapidly solidified melt. XRD did not reveal any differences in the unit cell parameters for silicate crystals in the fusion crust in comparison with the bulk material. However, XRD revealed chromite and hercynite, a twofold decrease of Fe-Ni-Co alloy and appearance of magnesioferrite as a result of metallic alloy and silicate combustion. Magnetization measurements showed the magnetic phase transitions for chromite around 48 and at ~21 K probably for hercynite while the saturation magnetic moment at 5 K was found to be 26 emu per g, which is twice smaller than that in the bulk material. The Mössbauer spectrum confirmed a decrease of Fe-Ni-Co alloy content and appearance of magnesioferrite in addition to components related to the M1 and M2 sites in silicate crystals, troilite, chromite, and yet unknown ferrous and ferric compounds. Based on the XRD and Mössbauer data, the temperature of the fusion crust final layer formation at the Ozerki L6 surface was estimated to be about 1000 K.

Acknowledgment—The authors are grateful to Dr. A. J. Timothy Jull for his useful remarks and comments which helped us to improve the manuscript. This work was supported by the Ministry of Science and Higher Education of the Russian Federation, the Project № 3.1959.2017/4.6 and by Act 211 of the Government of the Russian Federation, agreement № 02.A03.21.0006. M.G. acknowledges the Academy of Finland, project № 325806 (PlanetS) and the Russian Foundation for Basic Research, projects №s 18-08-00074 and 19-05-00028.

Editorial Handling—Dr. A. J. Timothy Jull

REFERENCES

De Grave E., Govaert A., Chambaere D., and Robbrecht G. 1979. A Mössbauer effect study of $MgFe_2O_4$. *Physica B* 96:103–110.

Elewa N. N. and Cadogan J. M. 2017. An ^{57}Fe Mössbauer study of the ordinary chondrite meteorite Lynch 001. *Hyperfine Interactions* 238:4.

Galazka-Friedman J., Wozniak M., Duda P., Rzepecka P., Jakubowska M., and Karwowski Ł. 2017. Mössbauer spectroscopy—A useful method for classification of meteorites? *Hyperfine Interactions* 238:67.

Gattacceca J., Rochette P., Lagroix F., Mathé P.-E., and Zanda B. 2011. Low temperature magnetic transition of chromite in ordinary chondrites. *Geophysical Research Letters* 38: L10203.

Gattacceca J., Suavet C., Rochette P., Weiss B. P., Winklhofer M., Uehara M., and Friedrich J. M. 2014. Metal phases in ordinary chondrites: Magnetic hysteresis properties and implications for thermal history. *Meteoritics & Planetary Science* 49:652–676.

Heinemann R., Staack V., Fischer A., Kroll H., Vad T., and Kirfel A. 1999. Temperature dependence of Fe, Mg partitioning in Acapulco olivine. *American Mineralogist* 84:1400–1405.

Klemme S. and Van Miltenburg J. C. 2003. Thermodynamic properties of hercynite ($FeAl_2O_4$) based on adiabatic calorimetry at low temperatures. *American Mineralogist* 88:68–72.

Lyytinen E. and Gritsevich M. 2016. Implications of the atmospheric density profile in the processing of fireball observations. *Planetary and Space Science* 120:35–42.

Maksimova A. A. and Oshtrakh M. I. 2019. Ordinary chondrites: What can we learn using Mössbauer spectroscopy? *Journal of Molecular Structure* 1186:104–117.

Maksimova A. A., Oshtrakh M. I., Klencsár Z., Petrova E. V., Grokhovsky V. I., Kuzmann E., Homonnay Z., and Semionkin V. A. 2014a. A comparative study of troilite in bulk ordinary chondrites Farmington L5, Tsarev L5 and Chelyabinsk LL5 using Mössbauer spectroscopy with a high velocity resolution. *Journal of Molecular Structure* 1073:196–201.

Maksimova A. A., Oshtrakh M. I., Petrova E. V., Grokhovsky V. I., and Semionkin V. A. 2014b. Study of Chelyabinsk LL5 meteorite fragment with light lithology and its fusion crust using Mössbauer spectroscopy with a high velocity resolution. In *Proceedings of the international conference "Mössbauer Spectroscopy in Materials Science 2014,"* edited by Tuček J. and Miglierini M. Melville, New York: AIP Conference Proceedings, Vol. 1622, pp. 24–29.

Maksimova A. A., Klencsár Z., Oshtrakh M. I., Petrova E. V., Grokhovsky V. I., Kuzmann E., Homonnay Z., and Semionkin V. A. 2016. Mössbauer parameters of ordinary chondrites influenced by the fit accuracy of the troilite component: An example of Chelyabinsk LL5 meteorite. *Hyperfine Interactions* 237:33.

Maksimova A. A., Oshtrakh M. I., Petrova E. V., Grokhovsky V. I., and Semionkin V. A. 2017. Comparison of iron-bearing minerals in ordinary chondrites from H, L and LL groups using Mössbauer spectroscopy with a high velocity resolution. *Spectrochimica Acta, Part A: Molecular and Biomolecular Spectroscopy* 172:65–76.

Maksimova A. A., Kamalov R. V., Chukin A. V., Felner I., and Oshtrakh M. I. 2018a. An analysis of orthopyroxene from Tsarev L5 meteorite using X-ray diffraction, magnetization measurement and Mössbauer spectroscopy. *Journal of Molecular Structure* 1174:6–11.

Maksimova A. A., Oshtrakh M. I., Chukin A. V., Felner I., Yakovlev G. A., and Semionkin V. A. 2018b. Characterization of Northwest Africa 6286 and 7857 ordinary chondrites using X-ray diffraction, magnetization measurements and Mössbauer spectroscopy. *Spectrochimica Acta, Part A: Molecular and Biomolecular Spectroscopy* 192:275–284.

Meteoritical Bulletin. 2018. No. 107. Ozerki. https://www.lpi.usra.edu/meteor/metbull.php?code = 67709

Malysheva T. V. 1975. *Mössbauer effect in geochemistry and cosmochemistry*. Moscow: Nauka. 166p. (in Russian).

Morozov M., Brinkmann C., Lottermoser W., Tippelt G., Amthauer G., and Kroll H. 2005. Octahedral cation partitioning in Mg, Fe^{2+}-olivine. Mössbauer spectroscopic study of synthetic $(Mg_{0.5}Fe^{2+}_{0.5})_2SiO_4$ (Fa50). *European Journal of Mineralogy* 17:495–500.

Oshtrakh M. I. and Semionkin V. A. 2013. Mössbauer spectroscopy with a high velocity resolution: Advances in biomedical, pharmaceutical, cosmochemical and nanotechnological research. *Spectrochimica Acta, Part A: Molecular and Biomolecular Spectroscopy* 100:78–87.

Oshtrakh M. I., and Semionkin V. A. 2016. Mössbauer spectroscopy with a high velocity resolution: Principles and applications. In *Proceedings of the international conference "Mössbauer Spectroscopy in Materials Science 2016,"* edited by Tuček J. and Miglierini M. Melville, New York: AIP Conference Proceedings, Vol. 1781, 020019.

Oshtrakh M. I., Petrova E. V., Grokhovsky V. I., and Semionkin V. A. 2008. A study of ordinary chondrites by Mössbauer spectroscopy with high-velocity resolution. *Meteoritics & Planetary Science* 43:941–958.

Oshtrakh M. I., Semionkin V. A., Milder O. B., and Novikov E. G. 2009. Mössbauer spectroscopy with high velocity resolution: An increase of analytical possibilities in biomedical research. *Journal of Radioanalytical and Nuclear Chemistry* 281:63–67.

Oshtrakh M. I., Maksimova A. A., Klencsár Z., Petrova E. V., Grokhovsky V. I., Kuzmann E., Homonnay Z., and Semionkin V. A. 2016. Study of Chelyabinsk LL5 meteorite fragments with different lithology using Mössbauer spectroscopy with a high velocity resolution. *Journal of Radioanalytical and Nuclear Chemistry* 308:1103–1111.

Oshtrakh M. I., Maksimova A. A., Chukin A. V., Petrova E. V., Jenniskens P., Kuzmann E., Grokhovsky V. I., Homonnay Z., and Semionkin V. A. 2019. Variability of Chelyabinsk meteoroid stones studied by Mössbauer spectroscopy and X-ray diffraction. *Spectrochimica Acta, Part A: Molecular and Biomolecular Spectroscopy* 219:206–224.

Paliwal B. S., Tripathi R. P., Verma H. C., and Sharma S. K. 2000. Classification of the Didwana-Rajod meteorite: A Mössbauer spectroscopic study. *Meteoritics & Planetary Science* 35:639–642.

Rubin A.E. 1997. Mineralogy of meteorite groups. *Meteoritics & Planetary Science*, 32, 231–247.

Sack R. O. and Ghiorso M. S. 1991. An internally consistent model for the thermodynamic properties of Fe-Mg-titanomagnetite-aluminate spinels. *Contributions to Mineralogy and Petrology* 106:474–505.

Semionkin V. A., Oshtrakh M. I., Milder O. B., and Novikov E. G. 2010. A high velocity resolution Mössbauer spectrometric system for biomedical research. *Bulletin of the Russian Academy of Sciences: Physics* 74:416–420.

Slater-Reynolds V. and McSween H. Y. Jr. 2005. Peak metamorphic temperatures in type 6 ordinary chondrites: An evaluation of pyroxene and plagioclase geothermometry. *Meteoritics & Planetary Science* 40:745–754.

Verma H. C. and Tripathi R. P. 2004. Anomalous Mössbauer parameters in the second generation regolith Ghubara meteorite. *Meteoritics & Planetary Science* 39:1755–1759.

Verma H. C., Rawat A., Paliwal B. S., and Tripathi R. P. 2002. Mössbauer spectroscopic studies of an oxidized ordinary chondrite fallen at Itawa-Bhopji, India. *Hyperfine Interactions* 142:643–652.

Verma H. C., Jee K., and Tripathi R. P. 2003. Systematics of Mössbauer absorption areas in ordinary chondrites and applications to newly fallen meteorite in Jodhpur, India. *Meteoritics & Planetary Science* 38:963–967.

Wang L., Moon N., Zhang Y., Dunham W. R., and Essene E. J. 2005. Fe-Mg order-disorder in orthopyroxenes. *Geochimica et Cosmochimica Acta* 69:5777–5788.

Yudin I. A., Kozmanov Yu D, and Remennikova I. M. 1968. Investigation of minerals in the fusion crust of Saratov meteorite. *Meteoritics (Moscow)* 28:156–157. (in Russian).

Zema M., Domeneghetti M. C., and Tazzoli V. 1999. Order-disorder kinetics in orthopyroxene with exsolution products. *American Mineralogist* 84:1895–1901.

SUPPORTING INFORMATION

Additional supporting information may be found in the online version of this article.

Fig. S1. Selected scanning electron microscopy images of the polished thin section of Ozerki L6 ordinary chondrite at different magnifications. Indicated phases were determined using energy dispersive spectroscopy.

Fig. S2. X-ray diffraction pattern of the bulk interior from Ozerki L6 ordinary chondrite. Ol = olivine, An = anorthite, OPy = orthopyroxene, CPy = clinopyroxene, Tr = troilite, Ch = chromite, Hc = hercynite, Cha is chlorapatite, α = α-Fe(Ni, Co) phase, γ = γ-Fe(Ni, Co) phase.

Fig. S3. Selected microphotographs of glass-like surface of the fusion crust at the polished thin section of Ozerki L6 ordinary chondrite obtained under nonpolarized (left) and polarized (right) light with high magnification.

Fig. S4. Scanning electron microscopy images of selected areas A and B of the fusion crust at the polished thin section of Ozerki L6 ordinary chondrite. Indicated phases were determined using energy dispersive spectroscopy.

Fig. S5. Scanning electron microscopy images of the glass-like surface of fusion crust at the polished thin section of Ozerki L6 ordinary chondrite at higher magnifications.